Development of Phase-Cycling Interface-Specific Two-Dimensional Electronic Sum Frequency Generation (2D-ESFG) Spectroscopy

Zhi-Chao Huang-Fu, Yuqin Qian, Tong Zhang, Jesse Brown, and Yi Rao*
Department of Chemistry and Biochemistry, Utah State University, Logan, UT84322
*Corresponding author: yi.rao@usu.edu

Abstract

Two-dimensional electronic spectroscopy (2D-ES) has become an important technique for studying energy transfer, electronic coupling, and electronic–vibrational coherence in the last ten years. However, since 2D-ES is not interface specific, the electronic information at surfaces and interfaces could not be demonstrated clearly. Two-dimensional electronic sum-frequency generation (2D-ESFG) is an emerging spectroscopic technique which explores the correlations between different interfacial electronic transitions and is the extension of 2D-ES to surface and interfacial specificity. In this work, we present the detailed development and implementation of phase-cycling 2D-ESFG spectroscopy using an acousto-optic pulse shaper in a pump-probe geometry. With the pulse pair generated by a pulse shaper rather than optical devices based on birefringence or interference, this 2D-ESFG setup enables rapid scanning, phase cycling, and the separation of rephasing and nonrephasing signals. Additionally, by collecting data in a rotating frame, we greatly improve experimental efficiency. We demonstrate the method for azo-derivative molecules at the air/water interface. This method could be readily extended to different interfaces and surfaces. The unique phase-cycling 2D-ESFG technique enables one to quantify energy transfer, charge transfer, electronic coupling, and many other electronic properties and dynamics at surfaces and interfaces with precision and relative ease of use. Our goal in this article is to present the fine details of the fourth-order nonlinear optical technique in a manner which is comprehensive, succinct, and approachable such that other researchers can implement, improve, and adapt it to probe unique and innovative problems to advance the field.

Introduction

Ultrafast multidimensional spectroscopy has been proven to be a robust tool to investigate chemical and physical processes of molecules.[1-4] These processes range from ultrafast intramolecular relaxation processes to intermolecular processes such as charge transfer, energy transfer, and electronic coupling in photochemical, biological, and materials systems[5-16] One such technique, two-dimensional electronic spectroscopy (2D-ES), has been very successful and used extensively to investigate ultrafast processes in bulk materials.[17-21] The great utility of 2D-ES is that by spreading the electronic spectrum into a second dimension, coupled electronic modes are correlated by cross peaks; and additional dynamical information can be derived from the 2D lineshapes.[22] However, since 2D-ES is not interface specific, electronic structure and dynamics at surfaces and interfaces cannot be clearly examined and separated from their dissimilar bulk

properties. As a second-order nonlinear optical technique, sum frequency generation (SFG) spectroscopy has been used to probe surfaces and interfaces because of the intrinsic surface/interface selectivity of even-order nonlinear processes.[23-26] Vibrational sum frequency generation (VSFG) have been proven to be a powerful tool to examine the vibrational information such as molecular structure, orientation, packing, and reactions at the interfaces.[27-40] To probe the electronic structures and photo-induced dynamics of molecules at interfaces, electronic sum frequency generation (ESFG) was developed and utilized.[41-49] By combining multidimensional and SFG spectroscopic methods, an interface-specific 2D spectroscopy could be developed, addressing this critical knowledge gap.

Time-resolved interfacial electronic spectroscopy has been used to study ultrafast interfacial processes such as solvation and rotational dynamics, electron, energy, and proton transfer, and excited state lifetimes. As far as photoinduced excited states are concerned, a UV-visible beam is used as a pump and ESHG or ESFG as a probe. Understanding these reactions using pump-probe spectroscopy would thus provide valuable mechanistic insights into a wide range of photoinduced relaxation processes at interfaces. Eisenthal and coworkers pioneered the time-resolved interfacial dynamics by developing time-resolved ESHG.[50] Specifically, the debut of time-resolved (TR) SHG showed that isomerization at the air/water interface could occur over twice as fast as in bulk. The team continued to expand the TR-ESHG to investigate unique solvation dynamics, rotational dynamics, and electron transfer at interfaces.[51-55] These works over 30 years ago ignited the field and have led to excellent innovations in ultrafast interfacial physical chemistry ever since.[43, 56, 57] The next major milestone in interfacial ultrafast electronic techniques was the use of a femtosecond 800 nm pulse mixed with a white light continuum to generate multiplex ESFG responses.[41, 44-46, 58, 59] Only a few years later Tahara et al. used the multiplex ESFG combined with a visible pump pulse to successfully mix three nondegenerate waves for the first time to investigate ultrafast interfacial dynamics through TR-ESFG.[60] Recently, the TR-ESFG technique was used to investigate interfacial organic chemical reactions at the air/water interface.[61, 62] Solid interfaces have been investigated using these techniques as well, where Zhu et al. used TR-ESHG to investigate charge transfer at organic/inorganic semiconductor interfaces.[63] Subsequently, with the addition of HD to the TR-ESFG system, they were able to probe interfacial charge transfer, charge carrier motion, as well as band normalization, all metrics imperative to the design and implementation of efficient semiconductors in photonics systems.[64] TR- and/or HD- ESHG/ESFG methods have been used to uncover interesting information about GaAs and GaP semiconductor surface properties.[57] Using ESFG, Zhang et al. were able to identify three dark surface states that contribute to band-bending in GaP semiconductors, and azimuthal angle-dependent phase measurements resulted in the correlation of surface charges and isotropic ESFG responses.[65] Along these lines, broadband HD-ESHG was used for spectral phase measurements for common nonlinear optical reference materials, both highlighting some serious pitfalls of common reference materials and providing a basis upon which they could be remedied.[66] Remarkably, the surface properties of GaP semiconductors have also been studied in-depth by broadband TR-ESFG, where surface states were identified for *n*- and *p*-type species, and their effects on surface electric fields and surface carrier population dynamics

at the material surface were assessed.[57, 67] Most recently, TR-ESFG observed the ultrafast charge transfer trions in 2D organometallic heterojunctions and was aided by phase differences in signal components, ultimately unveiling processes which may be useful in the improvement of designer photonic materials.[68] All these achievements in instrument development and interfacial knowledge advancements built on the previous work and instructed subsequent endeavors. Accordingly, the natural progression from ESFG to TR-/HD-ESFG was to combine it with two-dimensional spectroscopies.

Recently, two-dimensional vibrational SFG (2D-VSFG) spectroscopy has been demonstrated as an extension of two-dimensional infrared (2D-IR) techniques to study vibrational structures and dynamics at surfaces and interfaces.[69-74] By contrast, corresponding two-dimensional interface-specific electronic spectroscopy has still been left behind. One of the most challenging parts of developing a 2D-ESFG method is building up a broadband laser for an ESFG signal as a probe and a stabilized phase-locked visible pulse pair as a pump. In our previous work, we developed a broadband ESFG spectrometer based on an optical parametric amplifier that generates short-wave infrared (SWIR) from 1200 nm to 2400 nm.[49, 75, 76] The resultant ESFG spectrum covered almost all the visible light from 480 nm to 760 nm from mixing an 800 nm with the SWIR laser source. Based on this SWIR laser source, we developed 2D-ESFG and 2D-ESHG techniques with a phase-locked visible pulse pair from a Translating Wedge based Identical pulses eNcoding System (TWINS).[75-79] This suite of fourth-order nonlinear optical spectroscopic techniques allowed investigations of surface states for both *n*- and *p*-type GaAs surfaces. However, the TWINS-based 2D-ESFG spectroscopy system is not ideal for further development for multiple reasons. First, the time delay between two pump pulses at different wavelengths in the birefringent wedges was necessarily different and needed to be quantified. Second, precise 2D spectral analysis required the exact time-zero to be known. Third, an accurate and fine-step control of the phase-locked pulse is required to guarantee the accuracy of the measured excitation frequency; all of which contributed to very long sampling times of several hours. Last, any scattering from samples could introduce artifacts in the TWINS-based 2D-ESFG spectra.[80-84] As such, an alternative approach for efficient and reliable 2D-ESFG is needed.

Previously, a phase-cycling strategy was successfully employed in 2D-VSFG, where it showed utility in removing noise from scattering and separation of resonant and nonresonant responses to improve experimental quality and efficiency.[85] Phase-cycling and programmable control of pulse shapes allow precise and arbitrary control over the delay and phase for the pump pulses, which makes it possible to optimize the data acquisition and extend the experimental systems to rougher surfaces and air/water interfaces. Using a phase-cycling technique in 2D-SFG experiments can reduce sampling time and produce normalized, background-free data without the need for external calibration or validation. In this work, we detail the development of the 2D-ESFG spectroscopic method using a phase-cycling pulse shaper integrated into a visible-ESFG pump-probe geometry. As an example, we present the 2D-ESFG method on the couplings of molecules at the air/water interface. We believe that by providing an in-depth account of experimental development we can

make these advanced fourth-order nonlinear optical techniques more accessible to researchers who can apply them to their unique questions, and invite interested researchers to continue to improve the technology.

Experimental Section

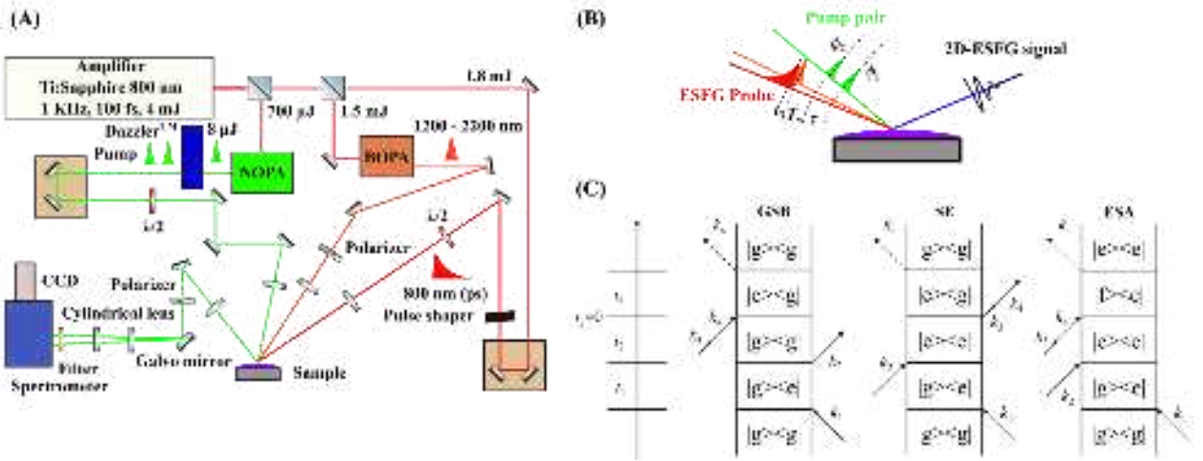

Figure 1. Schematic representation of (A) 2D-ESFG experimental setup and (B) the beam geometry and pulse sequence used for the 2D-ESFG experiments. (C) Double-sided Feynman diagrams (rephasing pathways) for a three-level system where |g>, |e> and |f> represent the ground state, the excited state, and a higher excited state, respectively. Nonrephasing pathways could be obtained by switching the time ordering of the first two interactions

Laser systems. As shown in Figure 1(A), the output from a Ti:Sapphire regenerative amplifier (Uptek Solution, 800 nm, 100 fs, ~4.0 mJ, 1 kHz repetition rate) was split into three beams to generate an 800 nm picosecond pulse, a SWIR pulse, and a visible pump pulse. The picosecond 800 nm pulse was produced by an etalon (SLS Optics), which allows simple switching back to a femtosecond pulse by removing the etalon. A portion of 1.5 mJ from the fundamental light pumped a two-stage broadband optical parametric amplifier (BOPA) to generate the SWIR pulse. A detailed description of the BOPA has been made in our previous work.[49, 75, 76] The BOPA was used to produce an ultra-broadband SWIR from 1200 to 2400 nm with a pulse energy of 250 μJ and a pulse duration of ~200 fs. A portion of 0.8 mJ from the fundamental light was used to pump a home-built non-collinear optical parametric amplifier (NOPA) tunable from 500 nm – 750 nm for the visible pump. The output of the NOPA (centered at 517 nm, full width at half maximum of 20 nm, 8.0 μJ) passed through an acousto-optic programmable dispersive filter pulse shaper (Dazzler, Fastlite) to generate the pump pulse pair with a relative phase and controllable delay for this work.[86, 87] The correction of high-order phase terms was achieved by the Dazzler for pulse compression of the pump. The pump pulse was characterized by a collinear phase-cycled SHG-FROG measurement with the Dazzler, resulting in a pulse duration of ~30 fs at the sample position.[88] The time delay between the picosecond 800 nm and the SWIR for generating ESFG was controlled by a programable motorized

translational stage (UT100-100, Klinger), and set to zero. Another programable motorized translational stage (ILS150BPP, Newport) / (M-112.12S Physik Instrumente) was used to control the time delay, T_w, between the pump pairs and the ESFG-generating pulses.

2D-ESFG Setup. A reflection geometry was used for ESFG and 2D-ESFG experiments, as shown in Figure 1(A) and (B), with all the pulses aligned non-collinearly into a single incident plane. The picosecond 800 nm pulse of 35 μJ was focused onto the sample surface with a 450 μm diameter spot (f=20.0 cm) at an angle of 60º. The SWIR of 5 μJ was focused on the sample surface with 150 μm diameter spot (f=15.0 cm) at an incident angle of 45°. The resultant ESFG spectrum covers the wavelength range of 475 – 550 nm. A 780 nm short-pass filter (Thorlabs) and a 445 nm long-pass filter (Thorlabs) were used to remove the fundamental light and stray light from the detection path. The 517 nm pump pair of 0.11 μJ was focused (f=25.0 cm) to a spot size of 250 μm at an incident angle of 37°, and spatially overlapped with the probe on the sample surface. The polarization combinations of ESFG/2D-ESFG signal, and incident pulses were controlled by polarizers (Thorlabs) and half-wave plates (Thorlabs), respectively. The polarizations of the pump pair, ESFG/2D-ESFG, 800-nm, and SWIR beams were set to be *p*, *s*, *s*, and *p*, respectively. *p* and *s* are defined to be parallel to and perpendicular to the incident plane, respectively.

The pulse-shaper can be used in various phase-cycling schemes, where two- and four-step schemes were used in our experiments. To eliminate the unwanted transient absorption background, a two-step (1×2) phase-cycling scheme whose signals were detected at relative phase differences $\phi_{12} = 0$ and $\phi_{12} = \pi$ was employed. An alternate two-step (1×2) phase-cycling scheme with $\phi_{12} = 0$ and $\phi_{12} = \pi/2$ can separate the rephasing and nonrephasing contributions using either a chopping or phase subtraction method. With the phase subtraction method, datasets were collected using a four-step (1×4) phase-cycling scheme. Here, $\phi_{12} = 0, \pi/2, \pi, 3\pi/2$, the subtraction between data at $\phi_{12} = 0$ and $\phi_{12} = \pi$ ($\phi_{12} = \pi/2$ and $\phi_{12} = 3\pi/2$) was used to remove pump-probe background and other ϕ_{12}-independent signals. Tan and coworkers showed that a three-step (1×3) phase-cycling scheme obtained the same data as this 1×4 phase-cycling scheme but with higher efficiency.[84] However, such a scheme is more difficult to be implemented in our current setup. Since 2D-ESFG signals are generally weak, each data point was acquired for 5 seconds, longer than the single-shot data collection used in most 2D experiments. The phase pattern for one cycle was uploaded to Dazzler and was repeated during data acquisition. At each waiting time, the 2D-ESFG spectra were acquired by scanning the coherence time. A 1 kHz trigger signal from the laser system was used for the synchronization of the Dazzler and a single-axis Galvo mirror (Thorlabs). The Galvo mirror rotated up and down at an angle of 1.5° and a frequency of 500 (250) Hz to separate the signals of the 1×2 (1×4) phase-cycling signals vertically into two (four) strips on the CCD chip. Andor Solis software from Andor Technology and a self-complied LabVIEW program were used to acquire data for the 2D-ESFG signals.

Chemicals. 10 μM [(E)-4-((4-(dihexylamino) phenyl)diazinyl)-1-methylpyridin-1-lum] (AP3) in water was used in our experiments. The chemical structure, synthesis, and characterization of AP3

were described in our early work.[77]

Results and Discussion

Like 2D-VSFG,[69, 85, 89-92]2D-ESFG is a fourth-order nonlinear spectroscopy where four pulses, including two visible pulses, one SWIR, and one ps 800 nm, generate a polarization that leads to the emission of interfacial responses. Explicitly, the two visible pulses form the phase-locked pump pulse pair, which interacts with the sample before the ESFG probe which is in resonance with an electronic mode of the sample. Figure 1 shows the beam geometry and pulse sequence used for the 2D-ESFG experiments in this work, as well as three Feynman rephasing pathways, including ground state bleaching (GSB), stimulated emission (SE), and excited state absorption (ESA). The experimental time delays of the laser pulses are the differences between the maxima of the pulse envelops, specified by coherent time (τ), population time (T_w), and ESFG time delay (t_3). The first field of E_{p1} with a phase, ϕ_1 and a wavevector, k_{p1} interacts with the sample initiating a coherent superposition of the ground and excited electronic states. The interaction of the second field of E_{p2} with a phase, ϕ_2 and a wavevector, k_{p2} leads to a population of either the ground or excited state. Then, the system is free to evolve during the waiting time T_w. After T_w, SWIR (E_{SWIR}) pulse with a wavevector of k_{SWIR} and a picosecond 800-nm beam, E_{ps} with a wavevector of k_{ps} are overlapped with a relative delay of t_3, and leading to the emission of the resultant 2D-ESFG signal at the temporal response t_4. The temporal response was measured in the frequency domain (λ_4) by a spectrometer coupled with a CCD. t_3 was set to be zero in our case. The direction of the radiated 2D-ESFG signal obeys the conservations of the energy and momentum ($\mp k_{p1} \pm k_{p2} + k_{ps} + k_{SWIR}$).

2D-ESFG in the rotating frame. Data acquisition in a rotating frame is a significant advantage of using a pulse shaper for our 2D-ESFG experiments.[81, 93] The emitted 2D-ESFG field, S_{2D}, depends on both τ and ϕ_{12}, and oscillates rapidly at ω, such that $S_{2D} \propto e^{i\omega\tau}e^{i\phi_{12}}$, where ω represents the frequency of the transition. To resolve coherent oscillations and to characterize the 2D signal, a sampling step in the time domain needs to be sufficiently small to acquire at least two samples during one optical cycle subject to the Shannon-Nyquist criterion. In our ESFG spectral region, this restricted a step size to be smaller than 1 fs (0.87 fs at 520 nm), which resulted in a long data collection time since nearly 200 data points are necessary to characterize the signal at a single T_w. To solve the problem, the coherent oscillations could be shifted to an arbitrary frequency or completely removed with a pulse shaper. Specifically, the time-domain carrier-envelope phase (CEP), ϕ_{CEP}, of a second pulse with respect to a first pulse is defined, namely, $\phi_{CEP}(\omega_0, \tau) = (1-\gamma_0)\omega_0\tau$, where ω_0 is the center frequency of the pump pulses, γ_0 is the adjustable parameter that controls the CEP evolution, and τ is the time delay of the two pulses. Thus, the carrier waves of the two pulses are kept in phase, while the CEP could be modulated by varying γ_0 and τ. During the scan of τ, the phase difference between two pump pulses is replaced by $\phi_{12} - \phi_{CEP}(\omega_0, \tau)$, then the acquired signal becomes $S_{2D} \propto e^{i(\omega-(1-\gamma_0)\omega_0)\tau}e^{i\phi_{12}}$, which oscillates at $\omega - (1-\gamma_0)\omega_0$. The sampling rate for the 2D line shape reconstruction at the

Nyquist-Shannon requirement could be tuned by γ_0.

To demonstrate how the rotating frame works, raw 2D-ESFG signals from air/10 μM AP3 solution interface with a waiting time of T_w = 1.8 ps at 19881 cm^{-1} (503 nm) were plotted as a function of coherence time, τ, as shown in Figure 2. When $\gamma_0 = 1$ (red line), the oscillations of the 2D-ESFG with the coherent time occur at the frequency of the transition. This is denoted as a laboratory-frame or no rotating frame measurements with no CEP shift between the two pulses. By contrast, for $\gamma_0 = 0$ (green line), the oscillations were shifted to the origin of the frequency space and oscillated with $\omega - \omega_0$, which is denoted as a fully rotating frame, showing a much lower

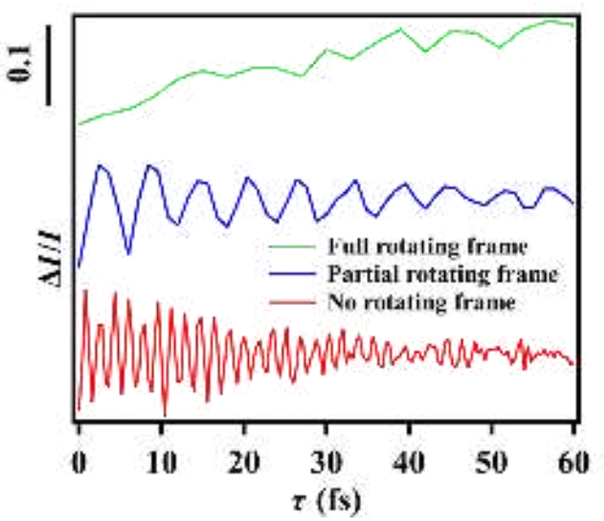

Figure 2. Raw 2D-ESFG signal as a function of coherence time τ at 19881 cm^{-1} (503 nm) from air/10 μM AP3 solution interface with a waiting time of T_w = 1.8 ps. Top ($\gamma_0 = 0$, green line), middle ($\gamma_0 = 0.3$, blue line), and bottom ($\gamma_0 = 1$, red line) correspond to fully, partially, and no rotating frame, respectively.

frequency. When $0 < \gamma_0 < 1$ (blue line, $\gamma_0 = 0.3$), the frequency of the oscillations was greatly reduced, which is denoted as a partially rotating frame. Considering the data collection time and noise levels at different frequencies, we used the sampling scheme in a partially rotating frame with $\gamma_0 = 0.15$ and 37 steps of τ evenly spaced between 0 and 90 fs in this work. The rotating frame greatly reduced the sample times to 5 minutes for 2D-ESFG measurement at each T_w, which is 10 times faster than those without the rotating frame.

Phase-cycling 2D-ESFG experiments. In our phase-cycling 2D-ESFG experiments, the frequency-resolved signal measured after a spectrometer is given by

$$S(\tau, T_w, t_3, \lambda_4) \propto \left| E^{(2)}(\lambda_4) + i\omega_4 \left[P^{(2)}(\lambda_4) + P^{(4)}_{S2D}(\tau, T_w, t_3, \lambda_4) + P^{(4)}_{p1}(\tau, T_w, t_3, \lambda_4) + P^{(4)}_{p2}(\tau, T_w, t_3, \lambda_4) \right] \right|^2, \quad \text{Eq. 1}$$

where $E^{(2)}(\lambda_4)$ is the ESFG probe field, $P^{(2)}(\lambda_4)$ is the free-induction decay from the ESFG

generated by the pulses 3 and 4, $P_{p1}^{(4)}$ and $P_{p2}^{(4)}$ are the polarization induced by the pump pulse 1 and 2, respectively. In other words, $P_{p1}^{(4)}$ and $P_{p2}^{(4)}$ are from pump-induced changes in ESFG. All three of these polarizations contribute to the strong background in the 2D-ESFG signal. $P_{S2D}^{(4)}$ is the desired 2D polarization induced by the interactions with all the pulses, which depends on the relative phase of the pump pulse pair of the form, $\phi_{12} = \phi_1 - \phi_2$. A Dazzler enables the independent phase and amplitude control over each pulse, which provides the ability to scan τ time delay and phase-cycling control.[94] Compared with the pulse pair produced by TWINS we used before or other interferometer setups,[75-77, 95-97] the pulse shaper employed here allows the introduction of an arbitrary carrier wave phase shift that could achieve specific phase-cycling schemes. We employed a 1×2 phase-cycling scheme of $\phi_{12} = 0$ and $\phi_{12} = \pi$ to obtain background-free 2D-ESFG signals. From Eq.1, changing the ϕ_{12} from 0 to π would change the phase of the 2D signal as well, but the pump-probe signal remained the same. The desired 2D signal could be isolated from other contributions by using a 1×2 phase-cycling. As a result, we are able to obtain only the isolated 2D-ESFG polarization.

$$S(\tau, T_w, t_3, \lambda_4; \phi_{12} = 0) - S(\tau, T_w, t_3, \lambda_4; \phi_{12} = \pi) \propto 2E^{(2)*}(\omega_4) P_{S2D}^{(4)}(\tau, T_w, t_3, \lambda_4) \qquad \text{Eq. 2}$$

Figure 3 shows the 2D-ESFG signals as a function of τ in a partially rotating frame for $\phi_{12} = 0$ (red curve) and $\phi_{12} = \pi$ (blue curve) at the probe wavelength of 19881 cm^{-1} (503 nm) with a

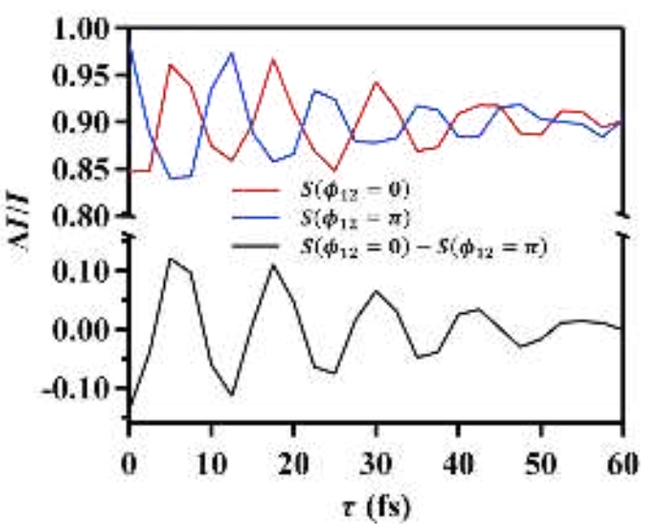

Figure 3. Raw 2D-ESFG signal as a function of coherence time τ at 19881 cm^{-1} (503 nm) in a two-step phase-cycling scheme with a partially rotating frame ($\gamma_0 = 0.15$) for ϕ_{12} = 0 (red line) and ϕ_{12} = π (blue line). The black line represents the signal difference of ϕ_{12}= 0 and ϕ_{12}= π.

waiting time of T_w =1.8 ps. Both curves show the oscillatory features with the offsets due to the pump-probe background polarizations ($P_{p1}^{(4)}$ and $P_{p2}^{(4)}$) as shown in Eq. 1. The black curve in the 2D difference signals for $\phi_{12} = 0$ and $\phi_{12} = \pi$ was enhanced without the background. Thus, this 1×2 phase-cycling scheme could remove the pump-probe background and enhance the desired 2D signal.

Obtaining purely absorptive 2D-ESFG spectra. From the detected photons to the desired 2D-ESFG signal, several steps need to be performed as schematically presented in Figure 4 (A), which is similar to the data processing of 2D-ES.[94]

Step 1: obtain the background-free signal by the subtraction, $S(\tau, T_w, t_3, \lambda_4) = S(\tau, T_w, t_3, \lambda_4; \phi_{12} = 0) - S(\tau, T_w, t_3, \lambda_4; \phi_{12} = \pi)$. Fourier transformation from wavelength domain needs the data as a function of equally spaced frequency, f_4. Therefore, a Jacobian transformation and a subsequent interpolation along the frequency axis are performed to extract $S(\tau, T_w, t_3, f_4)$.

Step 2: Since the pump pulses are essentially interchangeable for $\phi_{12} = 0$, the data must be symmetric with respect to $\tau = 0$ and therefore its Fourier transform along τ must be purely real; known as the symmetry condition. Experimentally, we obtained $S(\tau \geq 0, T_w, t_3, f_4)$ and applied the symmetry condition by performing the Fourier transform of $S(\tau \geq 0, T_w, t_3, f_4)$ along the τ axis and then the inverse Fourier transform of $\mathrm{Re}[S(f_1, T_w, t_3, f_4)]$ to determine $S(t_1, T_w, t_3, f_4)$.

Step 3: Subsequently, an inverse Fourier transform of $S(t_1, T_w, t_3, f_4)$ produces $S(t_1, T_w, t_3, t_4)$. Along the t_4 dimension, causality requires that there be no 2D signal if the probe pulse interacts with the sample before the pump pulses, which was enforced by setting the signal to zero for $t_4 < 0$.

Step 4: After applying the causality condition and taking the Fourier transform along both τ and t_4 axes into frequency domains, ν_1 and ν_4, we could obtain the complex absorptive 2D-ESFG spectrum $S(\nu_1, T_w, t_3, \nu_4)$. The real part of $S(\nu_1, T_w, t_3, \nu_4)$ is purely absorptive, and the imaginary part of it shows the dispersive spectrum.

Step 5: The use of a chirped continuum probe in 2D experiments leads to peak distortions that increase difficulties in analyzing the spectral and dynamical information. We obtained the cross-phase modulation (XPM) signal of the chirped ESFG probe with compressed pump pulse at the GaAs surface in the same configuration as the 2D-ESFG experiments. The time zero at each probe frequency could be determined. A post chirp-correction scheme for 2D experiments proposed by Ogilvie *et al.* was employed to correct the major distortions induced by chirped probe and give us the final 2D-ESFG spectra.[98]

Figure 4 (B) shows the real part of the absorptive 2D-ESFG spectrum of 10 μM AP3 solution at T_w = 0.030 ps. The negative diagonal peak at (19050 cm^{-1}, 19050 cm^{-1}) and off-diagonal peak at (19050 cm^{-1}, 18670 cm^{-1}) were assigned to ground state bleaching (GSB) and stimulated emission (SE), respectively. The elongated behavior along the diagonal direction is due to inhomogeneous broadening, while the spectral width in the antidiagonal direction reflects molecular homogeneous broadening effects. A 2D spectrum then enables us to correlate an excited frequency with a probe frequency. As a result, any inhomogeneous dephasing process that remains beyond its intrinsic homogeneous dephasing time will lead to a diagonally elongated 2D line shape. At the interfaces, a partial loss of frequency correlation with a symmetric line shape occurs at later waiting times due to environmental fluctuations. These spectral features suggest that i2D-ES spectra could be used to reveal spectral diffusion and correlations of electronic excited states of molecules at interfaces and surfaces.

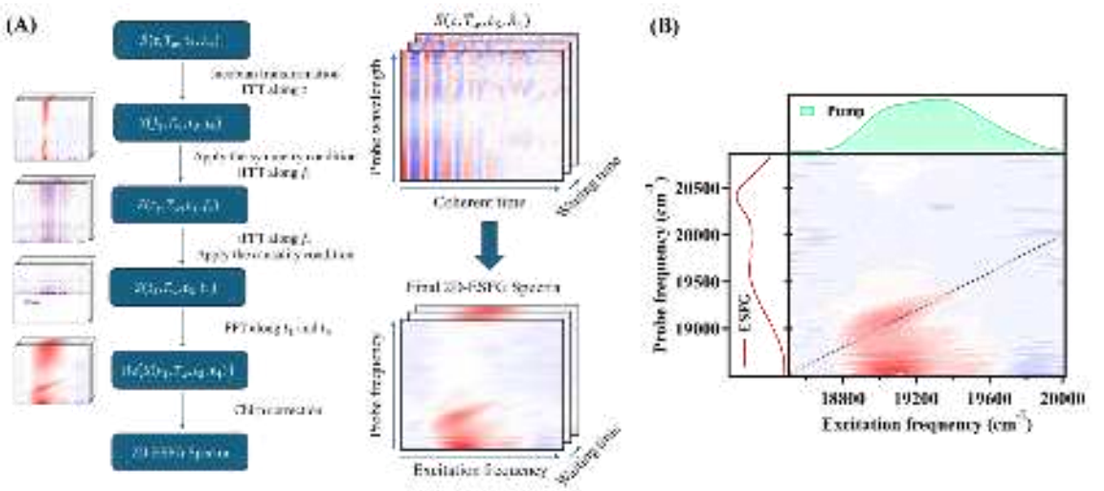

Figure 4. (A) A schematic of data processing in 2D-ESFG experiments. The raw 2D-ESFG data (three different T_w) are given on the top right, and after the five steps shown on the left end up with the final 2D-ESFG spectra on the bottom right. The results obtained after each step are shown on the side. (B) 2D-ESFG spectrum at T_w = 0.030 ps, with the pump spectrum (light-green shadow) and the ESFG intensity spectrum (red line).

The detected 2D signal in the pump-probe configuration is the sum of the rephasing (R) and nonrephasing (NR) signals, unlike the non-collinear geometries where R and NR signals are in different phase-matched directions and need to be detected separately. Ogilvie *et al.*[99] demonstrated that rephasing and nonrephasing 2D spectra could be isolated by employing a 1×2 phase-cycling scheme of $\phi_{12} = 0$ and $\phi_{12} = \pi/2$.[99] From Eq. 2, after the inverse Fourier transform along f_4, we obtain,

$$S(\phi_{12} = 0) \propto R^{(R)} + R^{(NR)}$$
$$S(\phi_{12} = \pi/2) \propto -iR^{(R)} + iR^{(NR)}. \quad \text{Eq. 3}$$

Then,

$$S(\phi_{12}=0)+iS(\phi_{12}=\pi/2)\propto R^{(R)}$$
$$S(\phi_{12}=0)-iS(\phi_{12}=\pi/2)\propto R^{(NR)}. \quad \text{Eq. 4}$$

Performing the combinations and taking the Fourier transform along both τ and t_4 axes can then give the 2D rephasing and nonrephasing spectra. In this work, we used a 1×4 phase-cycling scheme, $\phi_{12}=0,\pi/2,\pi,3\pi/2$, where four sets of data were collected. With an additional subtraction, background-free signals at $\phi_{12}=0$ and $\phi_{12}=\pi/2$ were obtained,

$$S(\phi_{12}=0)-S(\phi_{12}=\pi)\propto S(\phi_{12}=0)$$
$$S(\phi_{12}=\pi/2)-S(\phi_{12}=3\pi/2)\propto S(\phi_{12}=\pi/2). \quad \text{Eq. 5}$$

The two sets of signals could then provide the rephasing, nonrephasing, and purely absorptive 2D spectra. In Figure 5, we present the 2D-ESFG spectra of AP3 at 1.8 ps obtained from the 1×4 phase-cycling scheme. The three top panels show the real parts of rephasing and nonrephasing components as well as their sum that represents the purely absorptive 2D line shapes (left to right). The SE band elongated along the probe frequency is the major spectral feature, which is consistent with the spectral information obtained from the previous 1×2 phase-cycling scheme. We simulated the correlating 2D spectra based on perturbative expansion for comparison and reference,[100] as shown in the three bottom panels of Figure 5. The response function was modeled employing a two-level system with a vertical transition energy of 19200 cm^{-1}. The line broadening function g(t) was described by a Kubo lineshape function. The root-mean-square fluctuation Δ= 3500 cm^{-1} and the correlation time τ_c = 100 fs. The

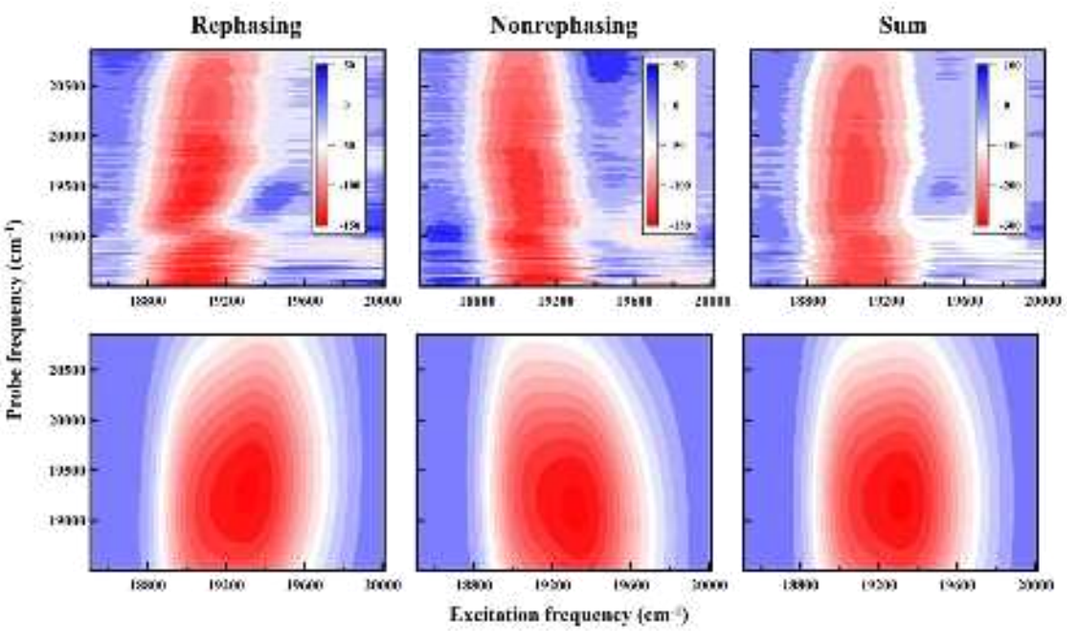

Figure 5. Experimental (top) and simulated (bottom) 2D-ESFG spectra (real parts) of 10 μM AP3 at 1.8 ps: rephasing (left) and nonrephasing (middle) as well as their sum (right).

shape of the pump pulse was also involved in the simulation. There are some differences between the experimentally observed spectra and simulated results because the relaxation process after the photo-excitation of the AP3 molecules at the interface is more complicated. Our previous studies have shown that a 590 nm pump could excite AP3 molecules to the optically bright S_2 state, followed by a conical intersection to the dark S_1 state. Molecules at either S_2 or S_1 state could give stimulated emission (SE) signals.[77, 101] With the higher energy 517 nm pump used in this work, the relaxation processes after photoexcitation are more complicated than a two-level system used in the simulation. From the experimental spectra, rephasing and nonrephasing components show differences in line shapes around probe frequency 19000 cm^{-1} and a slight shift along the excitation frequency. The individual analysis of both components could reveal the contributions from different coherent pathways, which is crucial for some systems. The spectral distortions at probe frequency 19000 cm^{-1} might come from the overlap of GSB and SE or pump scattering. Our future research focuses on improving this 2D-ESFG technique, including the introduction of some methods to suppress pump scattering.

Summary

In this work, we have detailed the development of phase-cycling 2D-ESFG spectroscopy with the goal of disseminating the technique to the community to expand its breadth of applicability. With the unique laser source of SWIR from 1200 nm to 2200 nm and the use of a phase-locked visible pump pulse pair from a pulse shaper, we demonstrated the advantages of the pulse shaper-based 2D-ESFG over the TWINS-based technique for interface/surface studies. We further extended the 2D-ESFG technique into the air/water interface. Due to relatively weak signal from the surfaces and interfaces, each step in a 2D-ESFG spectrum acquisition requires a certain time for averaging, but the use of a partially rotating frame allows for a significant reduction in the number of required data points per waiting time, reducing the overall acquisition time to more than one-fifth of that with the TWINs method. The more efficient acquisition and shorter collection time allowed for the tracking of ultrafast dynamics in amplitudes as well as line shapes of 2D-ESFG peaks with less effort from the user. In our technique, purely absorptive signals with no pump-probe background were retrieved using a 1×2 phase cycling scheme, along with retrieving rephasing and nonrephasing signals using a 1×4 phase cycling scheme. This additional spectral information enables efficient peak assignments and analysis of interfacial processes. We believe that our 2D-ESFG approach using a pulse shaper, due to its simplicity in operation, maintenance, and rich spectral information with different experimental settings, will make 2D-ESFG spectroscopy accessible to a wide range of interfacial systems, and reveal the electronic structure and dynamics of interfacial species in catalytic, environmental, and biological systems. By presenting the innerworkings of the phase-cycling 2D-ESFG process, we aim to provide a guideline by which other researchers can adopt, adapt, and improve the technique to best suit their own unique interests.

Acknowledgments

We acknowledge the supports from the National Science Foundation under Grant No.

[2045084].

Author contributions

*Corresponding author: yi.rao@usu.edu (Y.R)

References

[1] P. Hamm, M. Lim, F. DeGrado William, and M. Hochstrasser Robin, "The two-dimensional IR nonlinear spectroscopy of a cyclic penta-peptide in relation to its three-dimensional structure," Proc. Natl. Acad. Sci. U.S.A. **96** (1999) 2036.

[2] D. M. Jonas, "Two-Dimensional Femtosecond Spectroscopy," Annu. Rev. Phys. Chem. **54** (2003) 425.

[3] S. Park, K. Kwak, and M. D. Fayer, "Ultrafast 2D-IR vibrational echo spectroscopy: a probe of molecular dynamics," Laser Phys. Lett. **4** (2007) 704.

[4] L. P. DeFlores, R. A. Nicodemus, and A. Tokmakoff, "Two-dimensional Fourier transform spectroscopy in the pump-probe geometry," Opt. Lett. **32** (2007) 2966.

[5] T. Brixner, J. Stenger, H. M. Vaswani, M. Cho, R. E. Blankenship, and G. R. Fleming, "Two-dimensional spectroscopy of electronic couplings in photosynthesis," Nature **434** (2005) 625.

[6] J. M. Richter, F. Branchi, F. Valduga de Almeida Camargo, B. Zhao, R. H. Friend, G. Cerullo, and F. Deschler, "Ultrafast carrier thermalization in lead iodide perovskite probed with two-dimensional electronic spectroscopy," Nat. Commun. **8** (2017) 376.

[7] A. Jha, H.-G. Duan, V. Tiwari, P. K. Nayak, H. J. Snaith, M. Thorwart, and R. J. D. Miller, "Direct Observation of Ultrafast Exciton Dissociation in Lead Iodide Perovskite by 2D Electronic Spectroscopy," ACS Photonics **5** (2018) 852.

[8] G. S. Engel, T. R. Calhoun, E. L. Read, T.-K. Ahn, T. Mančal, Y.-C. Cheng, R. E. Blankenship, and G. R. Fleming, "Evidence for wavelike energy transfer through quantum coherence in photosynthetic systems," Nature **446** (2007) 782.

[9] F. D. Fuller, J. Pan, A. Gelzinis, V. Butkus, S. S. Senlik, D. E. Wilcox, C. F. Yocum, L. Valkunas, D. Abramavicius, and J. P. Ogilvie, "Vibronic coherence in oxygenic photosynthesis," Nature Chem. **6** (2014) 706.

[10] J. C. Dean, T. Mirkovic, Z. S. D. Toa, D. G. Oblinsky, and G. D. Scholes, "Vibronic Enhancement of Algae Light Harvesting," Chem **1** (2016) 858.

[11] A. A. Bakulin, S. E. Morgan, T. B. Kehoe, M. W. B. Wilson, A. W. Chin, D. Zigmantas, D. Egorova, and A. Rao, "Real-time observation of multiexcitonic states in ultrafast singlet fission using coherent 2D electronic spectroscopy," Nature Chem. **8** (2016) 16.

[12] Y. Lee, S. Das, R. M. Malamakal, S. Meloni, D. M. Chenoweth, and J. M. Anna, "Ultrafast Solvation Dynamics and Vibrational Coherences of Halogenated Boron-Dipyrromethene Derivatives Revealed through Two-Dimensional Electronic Spectroscopy," J. Am. Chem. Soc. **139** (2017) 14733.

[13] M. Alperstein Ariel, S. Ostrander Joshua, O. Zhang Tianqi, and T. Zanni Martin, "Amyloid found in human cataracts with two-dimensional infrared spectroscopy," Proc. Natl. Acad. Sci. U.S.A. **116** (2019) 6602.

[14] V. Tiwari, Y. A. Matutes, A. T. Gardiner, T. L. C. Jansen, R. J. Cogdell, and J. P. Ogilvie, "Spatially-resolved

fluorescence-detected two-dimensional electronic spectroscopy probes varying excitonic structure in photosynthetic bacteria," Nat. Commun. **9** (2018) 4219.

[15] T. A. A. Oliver, N. H. C. Lewis, and G. R. Fleming, "Correlating the motion of electrons and nuclei with two-dimensional electronic–vibrational spectroscopy," Proc. Natl. Acad. Sci. U.S.A. **111** (2014) 10061.

[16] T. L. Courtney, Z. W. Fox, K. M. Slenkamp, and M. Khalil, "Two-dimensional vibrational-electronic spectroscopy," J Chem Phys **143** (2015) 154201.

[17] P. Tian, D. Keusters, Y. Suzaki, and S. Warren Warren, "Femtosecond Phase-Coherent Two-Dimensional Spectroscopy," Science **300** (2003) 1553.

[18] G. S. Schlau-Cohen, A. Ishizaki, and G. R. Fleming, "Two-dimensional electronic spectroscopy and photosynthesis: Fundamentals and applications to photosynthetic light-harvesting," Chem. Phys. **386** (2011) 1.

[19] A. Halpin, P. J. M. Johnson, R. Tempelaar, R. S. Murphy, J. Knoester, T. L. C. Jansen, and R. J. D. Miller, "Two-dimensional spectroscopy of a molecular dimer unveils the effects of vibronic coupling on exciton coherences," Nature Chem. **6** (2014) 196.

[20] F. D. Fuller, and J. P. Ogilvie, "Experimental Implementations of Two-Dimensional Fourier Transform Electronic Spectroscopy," Annu. Rev. Phys. Chem. **66** (2015) 667.

[21] J. C. Dean, and G. D. Scholes, "Coherence Spectroscopy in the Condensed Phase: Insights into Molecular Structure, Environment, and Interactions," Acc. Chem. Res. **50** (2017) 2746.

[22] H. Seiler, S. Palato, C. Sonnichsen, H. Baker, E. Socie, D. P. Strandell, and P. Kambhampati, "Two-dimensional electronic spectroscopy reveals liquid-like lineshape dynamics in CsPbI3 perovskite nanocrystals," Nat. Commun. **10** (2019) 4962.

[23] X. D. Zhu, H. Suhr, and Y. R. Shen, "Surface vibrational spectroscopy by infrared-visible sum frequency generation," Phys Rev B Condens Matter **35** (1987) 3047.

[24] Y. R. Shen, "Surface-Properties Probed by 2nd-Harmonic and Sum-Frequency Generation," Nature **337** (1989) 519.

[25] Y. R. Shen, *Fundamentals of Sum-Frequency Spectroscopy* (Cambridge University Press, 2016),

[26] A. Morita, *Theory of sum frequency generation spectroscopy* (Springer, 2018), Vol. 97,

[27] K. B. Eisenthal, "Liquid interfaces probed by second-harmonic and sum-frequency spectroscopy," Chem. Rev. **96** (1996) 1343.

[28] M. J. Shultz, C. Schnitzer, D. Simonelli, and S. Baldelli, "Sum frequency generation spectroscopy of the aqueous interface: Ionic and soluble molecular solutions," Int. Rev. Phys. Chem. **19** (2000) 123.

[29] Z. Chen, Y. R. Shen, and G. A. Somorjai, "STUDIES OF POLYMER SURFACES BY SUM FREQUENCY GENERATION VIBRATIONAL SPECTROSCOPY," Annu. Rev. Phys. Chem. **53** (2002) 437.

[30] G. L. Richmond, "Molecular Bonding and Interactions at Aqueous Surfaces as Probed by Vibrational Sum Frequency Spectroscopy," Chem. Rev. **102** (2002) 2693.

[31] H.-F. Wang, W. Gan, R. Lu, Y. Rao, and B.-H. Wu, "Quantitative spectral and orientational analysis in surface sum frequency generation vibrational spectroscopy (SFG-VS)," Int. Rev. Phys. Chem. **24** (2005) 191.

[32] P. B. Petersen, and R. J. Saykally, "ON THE NATURE OF IONS AT THE LIQUID WATER SURFACE," Annu. Rev. Phys. Chem. **57** (2006) 333.

[33] F. M. Geiger, "Second Harmonic Generation, Sum Frequency Generation, and $\chi(3)$: Dissecting

Environmental Interfaces with a Nonlinear Optical Swiss Army Knife," Annu. Rev. Phys. Chem. **60** (2009) 61.

[34] A. M. Jubb, W. Hua, and H. C. Allen, "Environmental Chemistry at Vapor/Water Interfaces: Insights from Vibrational Sum Frequency Generation Spectroscopy," Annu. Rev. Phys. Chem. **63** (2012) 107.

[35] E. C. Y. Yan, L. Fu, Z. Wang, and W. Liu, "Biological Macromolecules at Interfaces Probed by Chiral Vibrational Sum Frequency Generation Spectroscopy," Chem. Rev. **114** (2014) 8471.

[36] H.-F. Wang, L. Velarde, W. Gan, and L. Fu, "Quantitative Sum-Frequency Generation Vibrational Spectroscopy of Molecular Surfaces and Interfaces: Lineshape, Polarization, and Orientation," Annu. Rev. Phys. Chem. **66** (2015) 189.

[37] F. Perakis, L. De Marco, A. Shalit, F. Tang, Z. R. Kann, T. D. Kühne, R. Torre, M. Bonn, and Y. Nagata, "Vibrational Spectroscopy and Dynamics of Water," Chem. Rev. **116** (2016) 7590.

[38] S. Nihonyanagi, S. Yamaguchi, and T. Tahara, "Ultrafast Dynamics at Water Interfaces Studied by Vibrational Sum Frequency Generation Spectroscopy," Chem. Rev. **117** (2017) 10665.

[39] A. Ge, B. Rudshteyn, P. E. Videla, C. J. Miller, C. P. Kubiak, V. S. Batista, and T. Lian, "Heterogenized Molecular Catalysts: Vibrational Sum-Frequency Spectroscopic, Electrochemical, and Theoretical Investigations," Acc. Chem. Res. **52** (2019) 1289.

[40] S. Hosseinpour, S. J. Roeters, M. Bonn, W. Peukert, S. Woutersen, and T. Weidner, "Structure and Dynamics of Interfacial Peptides and Proteins from Vibrational Sum-Frequency Generation Spectroscopy," Chem. Rev. **120** (2020) 3420.

[41] S. Yamaguchi, and T. Tahara, "Precise Electronic $\chi(2)$ Spectra of Molecules Adsorbed at an Interface Measured by Multiplex Sum Frequency Generation," J. Phys. Chem. B **108** (2004) 19079.

[42] C.-K. Lin, M. Hayashi, and S. H. Lin, "Theoretical Formulation and Simulation of Electronic Sum-Frequency Generation Spectroscopy," J. Phys. Chem. C **117** (2013) 23797.

[43] S. Yamaguchi, and T. Tahara, "Development of Electronic Sum Frequency Generation Spectroscopies and Their Application to Liquid Interfaces," J. Phys. Chem. C **119** (2015) 14815.

[44] Y. Li, J. Wang, and W. Xiong, "Probing Electronic Structures of Organic Semiconductors at Buried Interfaces by Electronic Sum Frequency Generation Spectroscopy," J. Phys. Chem. C **119** (2015) 28083.

[45] R. Pandey, A. P. Moon, J. A. Bender, and S. T. Roberts, "Extracting the Density of States of Copper Phthalocyanine at the SiO2 Interface with Electronic Sum Frequency Generation," J. Phys. Chem. Lett. **7** (2016) 1060.

[46] H. Mizuno, A. M. Rizzuto, and R. J. Saykally, "Charge-Transfer-to-Solvent Spectrum of Thiocyanate at the Air/Water Interface Measured by Broadband Deep Ultraviolet Electronic Sum Frequency Generation Spectroscopy," J. Phys. Chem. Lett. **9** (2018) 4753.

[47] B. R. Watson, B. Doughty, and T. R. Calhoun, "Energetics at the Surface: Direct Optical Mapping of Core and Surface Electronic Structure in CdSe Quantum Dots Using Broadband Electronic Sum Frequency Generation Microspectroscopy," Nano Lett. **19** (2019) 6157.

[48] L. Foglia, M. Wolf, and J. Stähler, "Ultrafast dynamics in solids probed by femtosecond time-resolved broadband electronic sum frequency generation," Appl. Phys. Lett. **109** (2016)

[49] G.-H. Deng, Y. Qian, and Y. Rao, "Development of ultrafast broadband electronic sum frequency generation for charge dynamics at surfaces and interfaces," J. Chem. Phys. **150** (2019) 024708.

[50] E. V. Sitzmann, and K. B. Eisenthal, "Picosecond dynamics of a chemical reaction at the air-water interface

studied by surface second harmonic generation," J. Phys. Chem. **92** (1988) 4579.

[51] D. Zimdars, J. I. Dadap, K. B. Eisenthal, and T. F. Heinz, "Anisotropic Orientational Motion of Molecular Adsorbates at the Air−Water Interface," J. Phys. Chem. B **103** (1999) 3425.

[52] D. Zimdars, and K. B. Eisenthal, "Static and Dynamic Solvation at the Air/Water Interface," J. Phys. Chem. B **105** (2001) 3993.

[53] X. Shang, K. Nguyen, Y. Rao, and K. B. Eisenthal, "In-Plane Molecular Rotational Dynamics at a Negatively Charged Surfactant/Aqueous Interface," J. Phys. Chem. C **112** (2008) 20375.

[54] E. A. McArthur, and K. B. Eisenthal, "Ultrafast Excited-State Electron Transfer at an Organic Liquid/Aqueous Interface," J. Am. Chem. Soc. **128** (2006) 1068.

[55] Y. Rao, S.-Y. Hong, N. J. Turro, and K. B. Eisenthal, "Molecular Orientational Distribution at Interfaces Using Second Harmonic Generation," J. Phys. Chem. C **115** (2011) 11678.

[56] T. Tahara, "Working on a dream: bringing up the level of interface spectroscopy to the bulk level," Bull. Chem. Soc. Jpn. **97** (2024)

[57] T. Zhang, J. B. Brown, H. Fisher, M. Liebes, Z.-C. Huang-Fu, Y. Qian, and Y. Rao, "Surface states of photoelectrodes by surface-specific steady-state and time-resolved sum frequency spectroscopies†," Chin. J. Chem. Phys. **37** (2024) 376.

[58] A. P. Moon, R. Pandey, J. A. Bender, D. E. Cotton, B. A. Renard, and S. T. Roberts, "Using Heterodyne-Detected Electronic Sum Frequency Generation To Probe the Electronic Structure of Buried Interfaces," J. Phys. Chem. C **121** (2017) 18653.

[59] N. Mirzajani, C. L. Keenan, S. R. Melton, and S. B. King, "Accurate phase detection in time-domain heterodyne SFG spectroscopy," Opt. Express **30** (2022) 39162.

[60] K. Sekiguchi, S. Yamaguchi, and T. Tahara, "Femtosecond time-resolved electronic sum-frequency generation spectroscopy: A new method to investigate ultrafast dynamics at liquid interfaces," J. Chem. Phys. **128** (2008) 114715.

[61] R. Kusaka, S. Nihonyanagi, and T. Tahara, "The photochemical reaction of phenol becomes ultrafast at the air–water interface," Nature Chem. **13** (2021) 306.

[62] C. J. C. Jordan, M. P. Coons, J. M. Herbert, and J. R. R. Verlet, "Spectroscopy and dynamics of the hydrated electron at the water/air interface," Nat. Commun. **15** (2024) 182.

[63] H. Park, M. Gutierrez, X. Wu, W. Kim, and X. Y. Zhu, "Optical Probe of Charge Separation at Organic/Inorganic Semiconductor Interfaces," J. Phys. Chem. C **117** (2013) 10974.

[64] C. A. Nelson, J. Luo, A. K. Y. Jen, R. B. Laghumavarapu, D. L. Huffaker, and X. Y. Zhu, "Time-, Energy-, and Phase-Resolved Second-Harmonic Generation at Semiconductor Interfaces," J. Phys. Chem. C **118** (2014) 27981.

[65] T. Zhang, Y. Qian, H. Gao, Z.-C. Huang-Fu, J. B. Brown, and Y. Rao, "Surface States for Photoelectrodes of Gallium Phosphide (GaP) with Surface-Specific Electronic Spectra and Phase Measurements," J. Phys. Chem. C **126** (2022) 6761.

[66] T. Zhang, Z.-C. Huangfu, Y. Qian, Z. Lu, H. Gao, and Y. Rao, "Spectral Phase Measurements of Heterodyne Detection in Interfacial Broadband Electronic Spectroscopy," J. Phys. Chem. C **126** (2022) 2823.

[67] T. Zhang, Z.-C. Huang-Fu, Y. Qian, H. Gao, J. B. Brown, and Y. Rao, "Photoinduced Surface Electric Fields and Surface Population Dynamics of GaP(100) Photoelectrodes," J. Phys. Chem. C **126** (2022) 6531.

[68] Y. Jing, K. Liang, N. S. Muir, H. Zhou, Z. Li, J. M. Palasz, J. Sorbie, C. Wang, S. K. Cushing, C. P. Kubiak,

Z. Sofer, S. Li, and W. Xiong, "Ultrafast Formation of Charge Transfer Trions at Molecular-Functionalized 2D MoS2 Interfaces," Angew. Chem. Int. Ed. **n/a** (2024) e202405123.

[69] J. Bredenbeck, A. Ghosh, M. Smits, and M. Bonn, "Ultrafast Two Dimensional-Infrared Spectroscopy of a Molecular Monolayer," J. Am. Chem. Soc. **130** (2008) 2152.

[70] S. Nihonyanagi, P. C. Singh, S. Yamaguchi, and T. Tahara, "Ultrafast Vibrational Dynamics of a Charged Aqueous Interface by Femtosecond Time-Resolved Heterodyne-Detected Vibrational Sum Frequency Generation," Bull. Chem. Soc. Jpn. **85** (2012) 758.

[71] P. C. Singh, S. Nihonyanagi, S. Yamaguchi, and T. Tahara, "Ultrafast vibrational dynamics of water at a charged interface revealed by two-dimensional heterodyne-detected vibrational sum frequency generation," J. Chem. Phys. **137** (2012) 094706.

[72] J. Wang, M. L. Clark, Y. Li, C. L. Kaslan, C. P. Kubiak, and W. Xiong, "Short-Range Catalyst–Surface Interactions Revealed by Heterodyne Two-Dimensional Sum Frequency Generation Spectroscopy," J. Phys. Chem. Lett. **6** (2015) 4204.

[73] E. B. Dunkelberger, M. Grechko, and M. T. Zanni, "Transition Dipoles from 1D and 2D Infrared Spectroscopy Help Reveal the Secondary Structures of Proteins: Application to Amyloids," J. Phys. Chem. B **119** (2015) 14065.

[74] W. Xiong, J. E. Laaser, R. D. Mehlenbacher, and M. T. Zanni, "Adding a dimension to the infrared spectra of interfaces using heterodyne detected 2D sum-frequency generation (HD 2D SFG) spectroscopy," Proc. Natl. Acad. Sci. U.S.A. **108** (2011) 20902.

[75] G.-H. Deng, Y. Qian, Q. Wei, T. Zhang, and Y. Rao, "Interface-Specific Two-Dimensional Electronic Sum Frequency Generation Spectroscopy," J. Phys. Chem. Lett. **11** (2020) 1738.

[76] G.-H. Deng, Q. Wei, Y. Qian, T. Zhang, X. Leng, and Y. Rao, "Development of interface-/surface-specific two-dimensional electronic spectroscopy," Rev. Sci. Instrum. **92** (2021) 023104.

[77] G.-H. Deng, Y. Qian, T. Zhang, J. Han, H. Chen, and Y. Rao, "Two-dimensional electronic–vibrational sum frequency spectroscopy for interactions of electronic and nuclear motions at interfaces," Proc. Natl. Acad. Sci. U.S.A. **118** (2021) e2100608118.

[78] D. Brida, C. Manzoni, and G. Cerullo, "Phase-locked pulses for two-dimensional spectroscopy by a birefringent delay line," Opt. Lett. **37** (2012) 3027.

[79] J. Réhault, M. Maiuri, A. Oriana, and G. Cerullo, "Two-dimensional electronic spectroscopy with birefringent wedges," Rev. Sci. Instrum. **85** (2014) 123107.

[80] R. Bloem, S. Garrett-Roe, H. Strzalka, P. Hamm, and P. Donaldson, "Enhancing signal detection and completely eliminating scattering using quasi-phase-cycling in 2D IR experiments," Opt. Express **18** (2010) 27067.

[81] S. K. K. Kumar, A. Tamimi, and M. D. Fayer, "Comparisons of 2D IR measured spectral diffusion in rotating frames using pulse shaping and in the stationary frame using the standard method," J. Chem. Phys. **137** (2012) 184201.

[82] W. Rock, Y.-L. Li, P. Pagano, and C. M. Cheatum, "2D IR Spectroscopy using Four-Wave Mixing, Pulse Shaping, and IR Upconversion: A Quantitative Comparison," J. Phys. Chem. A **117** (2013) 6073.

[83] H.-S. Tan, "Theory and phase-cycling scheme selection principles of collinear phase coherent multi-dimensional optical spectroscopy," J. Chem. Phys. **129** (2008) 124501.

[84] Z. Zhang, K. L. Wells, E. W. J. Hyland, and H.-S. Tan, "Phase-cycling schemes for pump–probe beam

geometry two-dimensional electronic spectroscopy," Chem. Phys. Lett. **550** (2012) 156.

[85] J. E. Laaser, W. Xiong, and M. T. Zanni, "Time-Domain SFG Spectroscopy Using Mid-IR Pulse Shaping: Practical and Intrinsic Advantages," J. Phys. Chem. B **115** (2011) 2536.

[86] P. Tournois, "Acousto-optic programmable dispersive filter for adaptive compensation of group delay time dispersion in laser systems," Opt. Commun. **140** (1997) 245.

[87] F. Verluise, V. Laude, Z. Cheng, C. Spielmann, and P. Tournois, "Amplitude and phase control of ultrashort pulses by use of an acousto-optic programmable dispersive filter: pulse compression and shaping," Opt. Lett. **25** (2000) 575.

[88] D. E. Wilcox, F. D. Fuller, and J. P. Ogilvie, "Fast second-harmonic generation frequency-resolved optical gating using only a pulse shaper," Opt. Lett. **38** (2013) 2980.

[89] A. Ghosh, M. Smits, J. Bredenbeck, N. Dijkhuizen, and M. Bonn, "Femtosecond time-resolved and two-dimensional vibrational sum frequency spectroscopic instrumentation to study structural dynamics at interfaces," Rev. Sci. Instrum. **79** (2008) 093907.

[90] E. H. G. Backus, J. D. Cyran, M. Grechko, Y. Nagata, and M. Bonn, "Time-Resolved Sum Frequency Generation Spectroscopy: A Quantitative Comparison Between Intensity and Phase-Resolved Spectroscopy," J. Phys. Chem. A **122** (2018) 2401.

[91] A. Ghosh, J.-J. Ho, A. L. Serrano, D. R. Skoff, T. Zhang, and M. T. Zanni, "Two-dimensional sum-frequency generation (2D SFG) spectroscopy: summary of principles and its application to amyloid fiber monolayers," Faraday Discuss. **177** (2015) 493.

[92] J. E. Laaser, D. R. Skoff, J.-J. Ho, Y. Joo, A. L. Serrano, J. D. Steinkruger, P. Gopalan, S. H. Gellman, and M. T. Zanni, "Two-Dimensional Sum-Frequency Generation Reveals Structure and Dynamics of a Surface-Bound Peptide," J. Am. Chem. Soc. **136** (2014) 956.

[93] S.-H. Shim, and M. T. Zanni, "How to turn your pump–probe instrument into a multidimensional spectrometer: 2D IR and Vis spectroscopiesvia pulse shaping," Phys. Chem. Chem. Phys. **11** (2009) 748.

[94] P. Tyagi, J. I. Saari, B. Walsh, A. Kabir, V. Crozatier, N. Forget, and P. Kambhampati, "Two-Color Two-Dimensional Electronic Spectroscopy Using Dual Acousto-Optic Pulse Shapers for Complete Amplitude, Phase, and Polarization Control of Femtosecond Laser Pulses," J. Phys. Chem. A **117** (2013) 6264.

[95] Z. C. Huang-Fu, Y. Qian, G. H. Deng, T. Zhang, S. Schmidt, J. Brown, and Y. Rao, "Development of Two-Dimensional Electronic-Vibrational Sum Frequency Generation (2D-EVSFG) for Vibronic and Solvent Couplings of Molecules at Interfaces and Surfaces," ACS Phys Chem Au **3** (2023) 374.

[96] Z. C. Huang-Fu, Y. Qian, T. Zhang, G. H. Deng, J. B. Brown, H. Fisher, S. Schmidt, H. Chen, and Y. Rao, "Orientational Coupling of Molecules at Interfaces Revealed by Two-Dimensional Electronic-Vibrational Sum Frequency Generation (2D-EVSFG)," JACS Au **3** (2023) 1413.

[97] J. Helbing, and P. Hamm, "Compact implementation of Fourier transform two-dimensional IR spectroscopy without phase ambiguity," J. Opt. Soc. Am. B **28** (2011) 171.

[98] P. A. Tekavec, K. L. M. Lewis, F. D. Fuller, J. A. Myers, and J. P. Ogilvie, "Toward Broad Bandwidth 2-D Electronic Spectroscopy: Correction of Chirp From a Continuum Probe," IEEE J. Sel. Top. Quantum Electron. **18** (2012) 210.

[99] J. A. Myers, K. L. M. Lewis, P. F. Tekavec, and J. P. Ogilvie, "Two-color two-dimensional Fourier transform electronic spectroscopy with a pulse-shaper," Opt. Express **16** (2008) 17420.

[100] S. Mukamel, *Principles of nonlinear optical spectroscopy* (Oxford University Press on Demand, 1999), 6

[101] Z. C. Huang-Fu, N. V. Tkachenko, Y. Qian, T. Zhang, J. B. Brown, A. Harutyunyan, G. Chen, and Y. Rao, "Conical Intersections at Interfaces Revealed by Phase-Cycling Interface-Specific Two-Dimensional Electronic Spectroscopy (i2D-ES)," J. Am. Chem. Soc. **146** (2024) 20996.